Topological braiding and virtual particles on the cell membrane

Jinghui Liu[a], Jan F. Totz[b,c], Pearson W. Miller[d], Alasdair D. Hastewell[b], Yu-Chen Chao[a,e], Jörn Dunkel[b,1], and Nikta Fakhri[a,1]

[a]Department of Physics, Massachusetts Institute of Technology, Cambridge, MA 02139; [b]Department of Mathematics, Massachusetts Institute of Technology, Cambridge, MA 02139; [c]Department of Mechanical Engineering, Massachusetts Institute of Technology, Cambridge, MA 02139; [d]Center for Computational Biology, Flatiron Institute, Simons Foundation, New York, NY 10010; and [e]School of Engineering and Applied Sciences, Harvard University, Cambridge, MA 02138

Edited by David A. Weitz, Harvard University, Cambridge, MA, and approved July 13, 2021 (received for review March 3, 2021)

Braiding of topological structures in complex matter fields provides a robust framework for encoding and processing information, and it has been extensively studied in the context of topological quantum computation. In living systems, topological defects are crucial for the localization and organization of biochemical signaling waves, but their braiding dynamics remain unexplored. Here, we show that the spiral wave cores, which organize the Rho-GTP protein signaling dynamics and force generation on the membrane of starfish egg cells, undergo spontaneous braiding dynamics. Experimentally measured world line braiding exponents and topological entropy correlate with cellular activity and agree with predictions from a generic field theory. Our analysis further reveals the creation and annihilation of virtual quasi-particle excitations during defect scattering events, suggesting phenomenological parallels between quantum and living matter.

braiding | topological defects | biochemical signaling waves | virtual particles | information transport

Braiding confers remarkable robustness to static and dynamic structures, from plaited hair and fabrics (1) to the entangled world lines of classical (2) and quantum particles (3). Stabilized by an inherent topological protection, braided threads, ropes, and wires have long been used to transmit forces and shield signals (4). Over the last decade, dynamic braiding processes (5–7) have attracted major interest in soft matter (8, 9) and quantum physics (3) as promising candidates for robust information storage and processing (10, 11). A widely studied application is topological quantum algorithms that perform computations by braiding the world lines of two-dimensional (2D) quasiparticle excitations (3, 10, 11). Of similar importance to information processing in living systems—albeit much less well understood—are the braiding dynamics of chemical spiral wave signals on cell membranes, which control a wide range of developmental and physiological functions, including cell division (12), cardiac rhythm (13–16), and brain activity (17). These spiral waves belong to a rapidly expanding class of recently discovered biological phenomena (18, 19) in which topological structures serve as robust organizers of essential life processes.

Similar to quantum states, biochemical spiral wave patterns can be described by complex wave functions (20), with spiral cores acting as topologically protected 2D quasiparticles (21). Although modern live-cell imaging now enables the direct observation of membrane spiral waves (22), their braiding dynamics have remained unexplored due to insufficient spatiotemporal resolution. Identifying the dynamic similarities and differences between 2D biochemical and quantum excitations poses a theoretically and practically relevant challenge, since optogenetic advances (23, 24) promise unprecedented control over cell signaling and hence biological computation. A particularly interesting open question in this context is whether fundamental quantum mechanical particle–particle interactions, symmetries (25), and scattering phenomena find counterparts in biological signaling processes. Our combined experimental and theoretical results below show that the self-braiding events of biochemical spiral wave cores on the cell membranes can exhibit virtual particle pair creation and annihilation and bosonic exchange symmetry, revealing profound parallels between defect dynamics and information transport in living and quantum matter.

Driven by recent experimental progress (18, 22, 26–28), the exploration of topological defects in synthetic and natural active matter has become a rapidly expanding area of research (29–38). In living systems, energy conversion of ATP at the microscale leads to the emergence of complex biochemical and biophysical signaling patterns at the mesoscale and macroscale (22, 27, 39). Such nonequilibrium patterns often display rich topological textures and dynamics (32, 33, 40, 41), arising from the defects' self-propulsion (29) and interactions (30, 31). Owing to their robustness and slow dynamics, topological excitations can act as stabilizers and organizers of active force generation (18), biological functions (19), and information flows. Recent work determined the topological entropy associated with the braiding of defects in active nematic liquid crystals (37). By contrast, the relation between spontaneous topological defect braiding and information loss in

Significance

Topological defects are robust particle-like structures that essentially determine the mechanics and dynamics of physical and biological matter. Examples range from vortices in quantum superfluids to the cores of spiral wave patterns in the brain. In biological systems, such defects play important roles as organizers of biochemical signaling patterns, cellular forces, and even cell death. Combining direct experimental observations with mathematical modeling and chemical perturbations, we investigated the dynamics of spiral wave defects on the surfaces of starfish egg cells. Our quantitative analysis showed that these defects exhibit complex braiding, pair creation, and annihilation dynamics, in agreement with predictions from a generic continuum theory. More broadly, these results suggest interesting parallels between information transport in living and quantum systems.

Author contributions: J.D. and N.F. designed research; J.L., J.F.T., P.W.M., A.D.H., and Y.-C.C. performed research; J.L., J.F.T., P.W.M., and A.D.H. contributed new reagents/analytic tools; J.L., J.F.T., and A.D.H. analyzed data; and J.L., J.F.T., P.W.M., A.D.H., Y.-C.C., J.D., and N.F. wrote the paper.

The authors declare no competing interest.

This article is a PNAS Direct Submission.

[1]To whom correspondence may be addressed. Email: dunkel@mit.edu or fakhri@mit.edu.

This article contains supporting information online at https://www.pnas.org/lookup/suppl/doi:10.1073/pnas.2104191118/-/DCSupplemental.

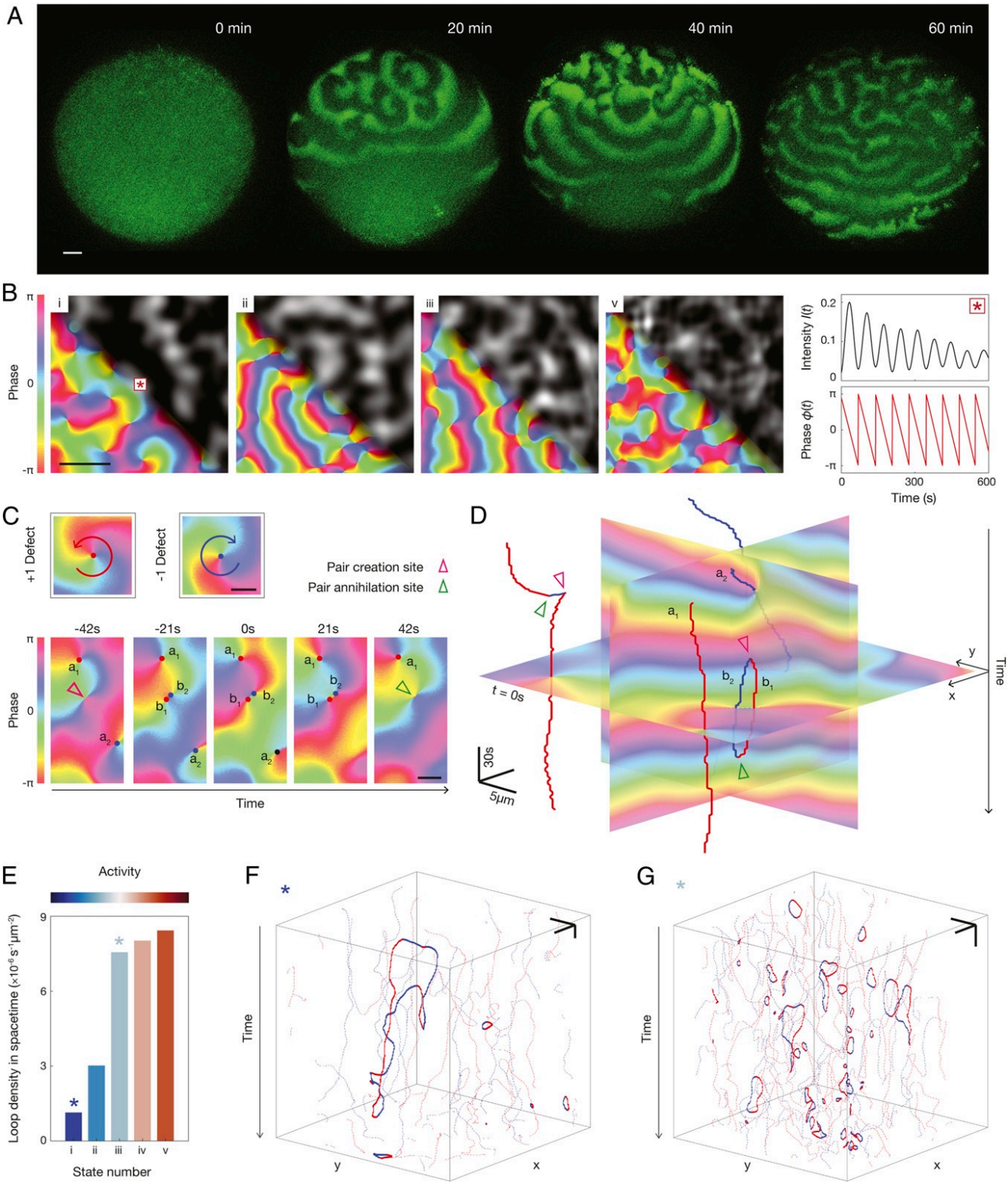

Fig. 1. Direct measurement of defect world line dynamics during membrane signaling wave propagation. (*A*) Time evolution of chemical Rho signaling wave patterns on the starfish oocyte from a homogeneous initial state to a quasi-steady state exhibiting turbulent spiral patterns. Snapshots show maximal intensity projections of three near-membrane Z-stack confocal slices spanning 5 μm (Movie S1). (Scale bar: 40 μm.) (*B*) Quasi-steady wave patterns ($t > 60$ min) of Rho-GTP intensity field from four starfish egg cells, aligned with phase fields reconstructed from oscillations in pixel fluorescence intensity signal (*Right*). (Scale bar: 20 μm.) Five wave propagation states on five different egg cells were analyzed in total (Movies S2–S6). (*C*) The reconstructed phase fields harbor topological defects of winding number +1 (red, counterclockwise rotating spiral core) and −1 (blue, clockwise rotating spiral core) (*Upper*). Time-lapse snapshots of localized creation (annihilation) events that produce (destroy) oppositely charged defects in pairs (*Lower*). (Scale bar: 5 μm.) (*D*) World line representation of topological defects embedded in 2+1-dimensional phase field. The time-lapse snapshots in *C* correspond to formation of the simple space—time loop in *D*. (Scale bars: 5 μm; 30 s [vertical] [Movie S7]). (*E*) Loop density characterizes signaling waves from five different oocytes (states i to v) varying in cellular activity. Asterisks annotate the lower-activity and higher-activity state i and iii, as presented next in *F* and *G*. (*F*) Space—time defect loops from experimental wave state i (lower activity). (Scale bars: 10 μm; 90 s [vertical]). (*G*) Space—time defect loops from experimental wave state iii (higher activity). (Scale bars: 10 μm; 90 s [vertical]).

cell membrane signaling processes (22) has remained relatively unexplored.

To investigate the braiding dynamics of biochemical spiral waves in living cells, we compared here experimental observations of Rho-GTP activation waves on starfish oocyte membranes (22) with predictions of a generic continuum theory (20). Rho-GTP is a highly conserved signaling protein pivotal in regulating cellular division (42) and mechanics (43) across a wide variety of eukaryotic species (44). Since the biological functions of Rho-GTP have been widely investigated previously (45), we focused here on the topological characterization of the biochemical signaling dynamics through braiding analysis of defect world lines and entropic information measures, to identify similarities and differences with wave propagation and particle scattering dynamics in quantum systems. Overcoming previous observational and algorithmic limitations, we achieved the spatiotemporal resolution required for dynamical analysis by combining in vivo imaging with spectral signal representation, quantitative mathematical modeling, and large-scale computational parameter estimations (*Materials and Methods*) (46).

Results

Topological Defect Dynamics in Rho-GTP Signaling Patterns. To visualize the self-organized Rho-GTP wave patterns on the membrane of the oocytes (45), we used the enhanced green fluorescent protein/rhotekin GTPase binding domain (eGFP-rGBD) biosensor (Fig. 1*A* and *SI Appendix*, Fig. S1 and Movie S1). Different steady-state patterns of Rho-GTP were induced by a systematic increase of the GEF (guanine exchange factor) responsible for activating Rho-GTP (states i to v) (39). Rho-GTP waves maintained constant oscillatory periods within all observed nonequilibrium steady states with different cellular activity (22) (Movies S2–S6), enabling the reconstruction of spatiotemporal phase fields (Fig. 1*B* and *SI Appendix*, Fig. S2 and *Materials and Methods*). Topological defects in the phase field are singular points with winding number $+1$ or -1 corresponding to counterclockwise or clockwise rotating centers of propagating spiral waves (Fig. 1*C*). These phase defects are created and annihilated in pairs, conserving the total topological charge (Fig. 1*C*). By tracking the $2+1$-dimensional world lines of both defect types, we observed complex creation, annihilation, and braiding dynamics (Fig. 1*D*), similar to those in Bose–Einstein condensates (46, 47) (Movie S7). Closed space–time loops (*SI Appendix*, Fig. S3) reflect successive defect pair creation and annihilation events. Rho-GTP spiral waves from the five observed oocytes exhibited varying densities of space–time defect loops, reflecting differences in cellular activity (Fig. 1*E*). Despite such quantitative variations, all signaling patterns displayed a wide range of loop structures and sizes (Fig. 1 *F* and *G* and *SI Appendix*, Fig. S3). Steady-state spiral waves of low-activity oocytes (Fig. 1*F*) exhibited a lower loop density compared with high-activity cells (Fig. 1*G*). To confirm the link between cellular activity and defect loop statistics,

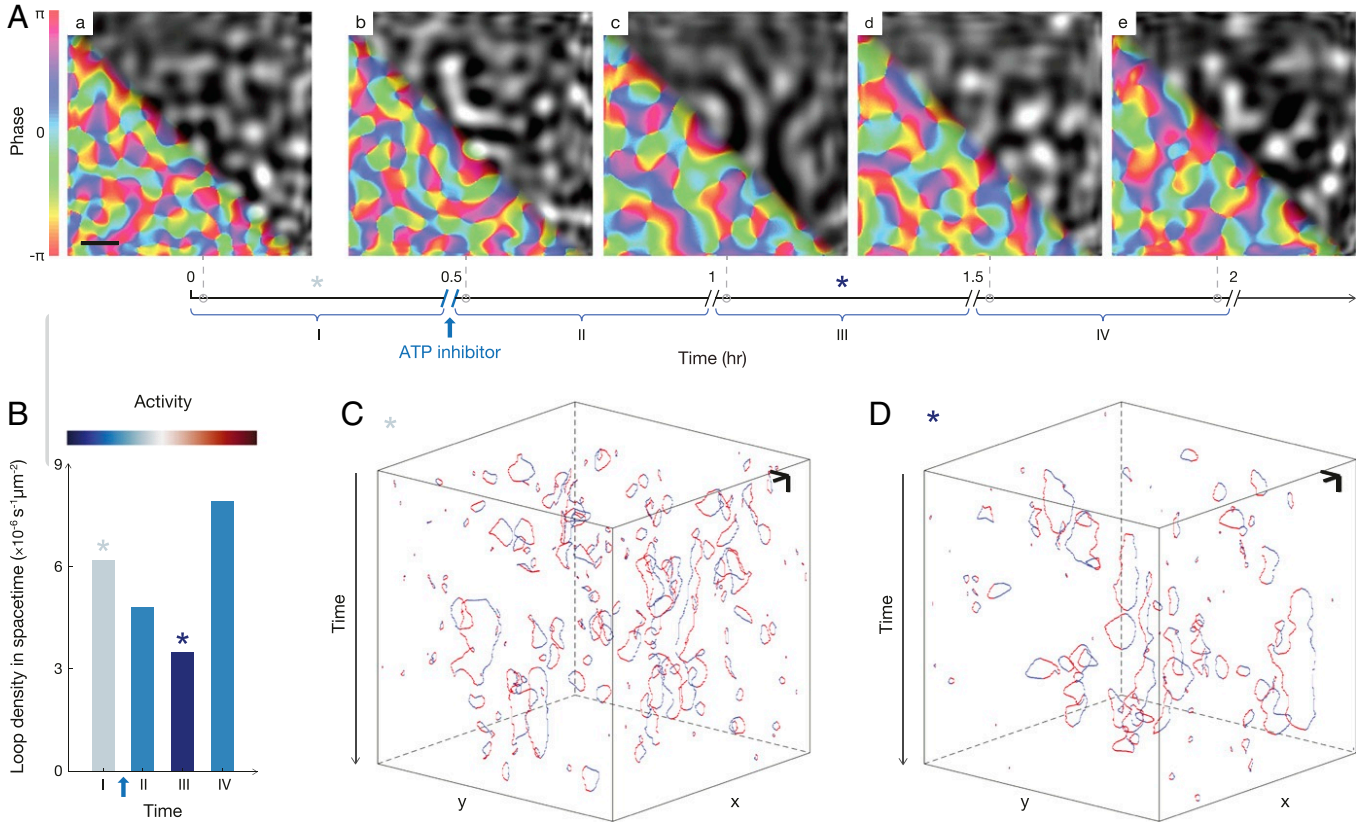

Fig. 2. ATP depletion induces structural changes in the membrane signaling patterns and reduces the frequency of topological defect creation and annihilation events. (*A*) Time evolution of Rho-GTP intensity field and phase field from a starfish egg cell treated with ATP depletion drug sodium azide (*Materials and Methods* and Movie S8). Videos I through IV in Movie S8 each has a duration of 30 min and were taken sequentially, separated by short (<3 min) intervals in between. The drug treatment was performed after video I and before the start of video II. (Scale bars: 20 μm.) Asterisks denote the pretreatment video I and posttreatment video III, as presented next in *B*–*D*. (*B*) Loop density as a function of time showing a transient drop in cellular activity in response to the ATP depletion treatment. (*C*) Space–time defect loops before ATP depletion recorded during phase I in *A*. (Scale bars: 10 μm; 90 s [vertical]). (*D*) After ATP depletion (phase III in *A*), the density of space–time defect loops decreases significantly, reflecting the reduction of cellular activity. (Scale bars: 10 μm; 90 s [vertical]).

we performed additional experiments, in which starfish oocytes exhibiting steady-state wave patterns were perturbed with the ATP-depleting drug sodium azide (*Materials and Methods* and Fig. 2). After exposure to the drug, the Rho-GTP concentration patterns (Movie S8) and their associated phase fields displayed visible structural and dynamical changes (Fig. 2*A*): Over a period of ∼1 h, the space–time loop densities decreased, reflecting the decrease in cellular activity, before eventually returning to preperturbed levels (Fig. 2 *B–D* and *SI Appendix*, Fig. S3). These observations are consistent with the previous measurements for steady-state cells (Fig. 1 *B* and *E–G*), supporting the hypothesis that cellular activity and topological defect dynamics are linked.

Defect Braiding Dynamics. In addition to short-lived loops which dominate at high activity, low-activity states (Fig. 1 *B*, *i–iii*) exhibit a large number of long-lived defect world lines that undergo spontaneous braiding dynamics (Fig. 3*A*). Space–time braiding of spiral cores is indicative of chaotic dynamics of the Rho-GTP signaling patterns. To quantify the associated topological entropy increase, we classified braiding events by adopting the reduced Burau matrix representation of the n-particle braid group (48). To this end, we first identified elementary braiding events from the crossing of projected world lines (Fig. 3*A*). Each clockwise or counterclockwise braiding event n is then represented by a $(n-1)\times(n-1)$ matrix $\sigma^{(n)}\in\{\sigma_i,\sigma_i^{-1}\}$, where the σ_i are the generators of Burau representation (*Materials and Methods*). Accordingly, a sequence of $n=1,\ldots,N$ successive braiding events is encoded by the matrix product $\Sigma^{(N)}=\sigma^{(N)}\sigma^{(N-1)}\ldots\sigma^{(1)}$ of the corresponding elementary generators (2). The largest eigenvalue Λ of the braid matrix $\Sigma^{(N)}$, known as the braiding factor, determines the braiding exponent $\lambda=(1/t)\log\Lambda$, which measures the growth rate of the topological entropy in chaotic systems (2).

Braiding Exponents and Topological Entropy. To calculate the braiding exponents λ from our experimental data (6), we constructed a library of long-lived $+1$ and -1 defect world lines for the low-activity signaling states i, ii, and iii (Fig. 3*A* and *Materials and Methods*). Braiding exponents for different defect numbers were then computed and averaged across subgroups of world lines bootstrapped from the library (*SI Appendix*, Figs. S4 and S5 and *Materials and Methods*). Our evaluation

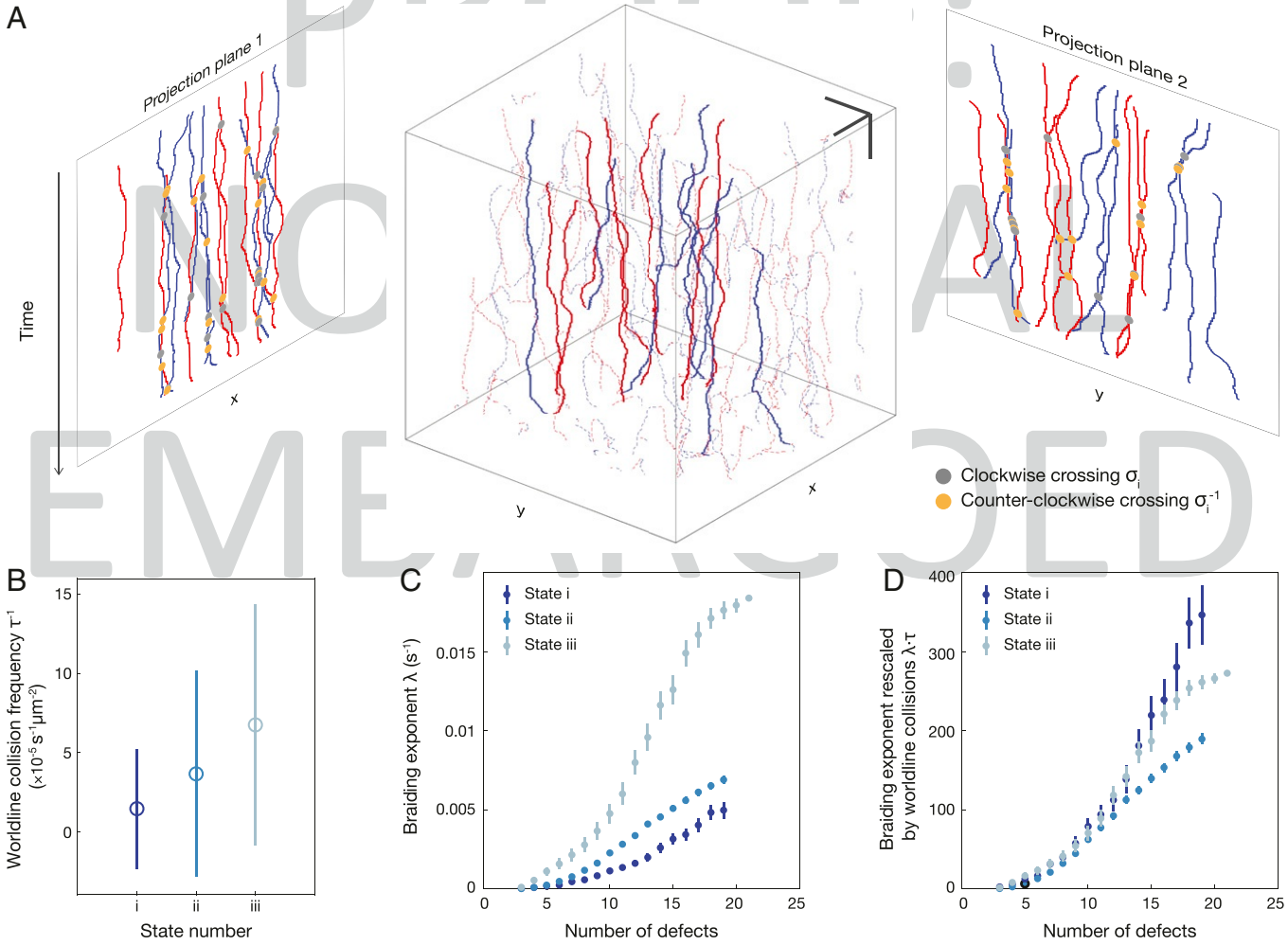

Fig. 3. Spontaneous braiding of topological defects and world line collisions during cell signaling. (*A*) Representative selection of braided defect world lines from low-activity state i. Braiding dynamics are quantified by multiplying braiding operators (σ_i, σ_i^{-1}) and averaging over a collection of projected world line cross-overs (*Materials and Methods* and *SI Appendix*, Fig. S4). (Scale bars: 20 μm; 240 s [vertical]). (*B*) World line collision (defect pair creation and annihilation) frequencies per unit area for states i, ii, and iii exhibit a sequential rise. Error bars represent SD throughout time. (*C*) Measured braiding exponents as a function of total defect number exhibit a sequential rise in magnitude with increasing activities from states i to iii. Error bars represent SE across bootstrap samples. (*D*) Braiding exponents from *C* collapse when rescaled by the world line collision frequencies. Error bars represent SE across bootstrap samples.

of world line collision frequencies reveals different time scales of cellular activities across signaling wave states (Fig. 3*B*). The estimated braiding exponents support the hypothesis that topological entropy increases faster at higher cellular activity (Fig. 3*C*). When rescaled by the world line collision frequencies τ^{-1}, the braiding exponents collapse onto a single curve (Fig. 3*D*). This result presents a direct link between the spontaneous topological braiding of spiral defects and information loss in the cellular signaling waves.

Discussion

Quantitative Mapping to a Complex Ginzburg–Landau Theory. To understand whether the above results translate to a broader class of biochemical signaling systems, we compared the experimentally observed loop and braiding dynamics with predictions from a generic spiral wave theory (20). We simulated a complex Ginzburg–Landau (CGL) continuum model (20, 49) with tunable levels of activity (Fig. 4*A* and *SI Appendix*, Fig. S6). The CGL theory describes a general class of nonlinear waves capable of embedding spiral cores, for which effective diffusion and reaction parameters can be systematically derived as combinations of constants from a multispecies reaction–diffusion system (*SI Appendix*, Figs. S7 and S8 and *Materials and Methods*). By tuning the reaction parameter in the CGL model, we were able to quantitatively match the CGL phase field dynamics to the oocyte states i, ii, and iii in both space (Fig. 4*A* and *SI Appendix*, Fig. S9) and time (Fig. 4 *B* and *C*, Movie S9, and *Materials and Methods*). Detailed braiding analysis of the space–time defect dynamics of CGL states confirmed that higher-activity states show faster topological entropy growth (Fig. 4*D*). In agreement with our experimental observations, the braiding exponents collapse when rescaled by the world line collision frequencies (Fig. 4*E*). Taken together, these results support the conclusion that essential aspects of wave-mediated information processing on the oocyte membrane can be modeled and studied within a generic CGL theory framework.

Virtual Quasi-particle Excitations on the Cell Membrane. Macroscopic information loss in spiral wave signaling patterns results from the microscopic interactions between the defect cores. Future efforts to control biochemical membrane signaling through optogenetic intervention will thus require a detailed understanding of microscopic defect scattering events. We therefore applied our analysis framework to study the previously inaccessible short-range defect scattering dynamics. While two colliding opposite-sign spiral cores tend to annihilate, a pair of interacting same-sign spiral cores can exhibit intricate dynamics (Fig. 5). In addition to basic pair-braiding dynamics (Fig. 5*A* and Movie S10), our data revealed scattering events during which short-lived "virtual" particles were created (Fig. 5 *B* and *C*). Such virtual particles annihilated either mutually (Fig. 4*B* and Movie S10) or by recombination with one of the original defects (Fig. 5*C* and Movie S10). These biochemical scattering events have known counterparts in quantum systems (50), and all of them can also be identified in the corresponding CGL wave states (Fig. 5, *Lower*). Another interesting parallel with quantum systems relates to the pair exchange symmetry when two equal-sign spiral defects exchange positions through braiding. In the case of two identical quantum particles, the global phase shift acquired

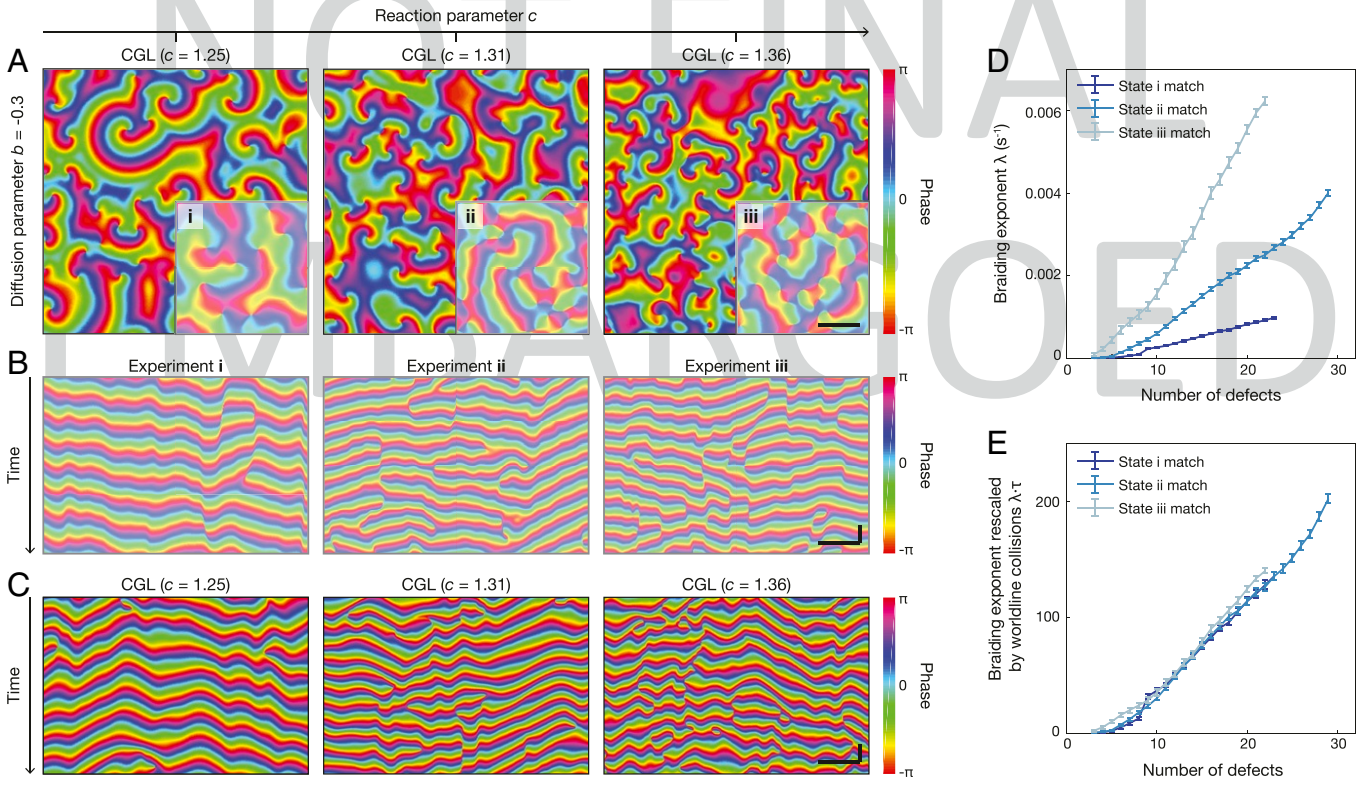

Fig. 4. A generic CGL model captures phase continuum and defect-braiding dynamics with tunable activity. (*A*) Representative snapshots comparing phase fields of best-fit (*Materials and Methods*) CGL (49) models with oocyte states i, ii, and iii (*Insets*), animated in Movie S9. (Scale bar: 20 μm.) (*B*) Snapshots of space–time slices (kymographs) for states i, ii, and iii, animated in Movie S9. (Scale bar: 20 μm; 50 s [vertical]). (*C*) Snapshots of space–time slices (kymographs) for CGL matches of states i, ii, and iii, animated in Movie S9. (Scale bar: 20 μm; 50 s [vertical]). (*D*) Braiding exponents as a function of total defect number exhibit a similar sequential rise in magnitude across CGL matches of states i, ii, and iii. Error bars represent SE across bootstrap samples. (*E*) Braiding exponent curves across CGL matches from *D* consistently collapse when rescaled by the world line collision frequencies. Error bars represent SE across bootstrap samples.

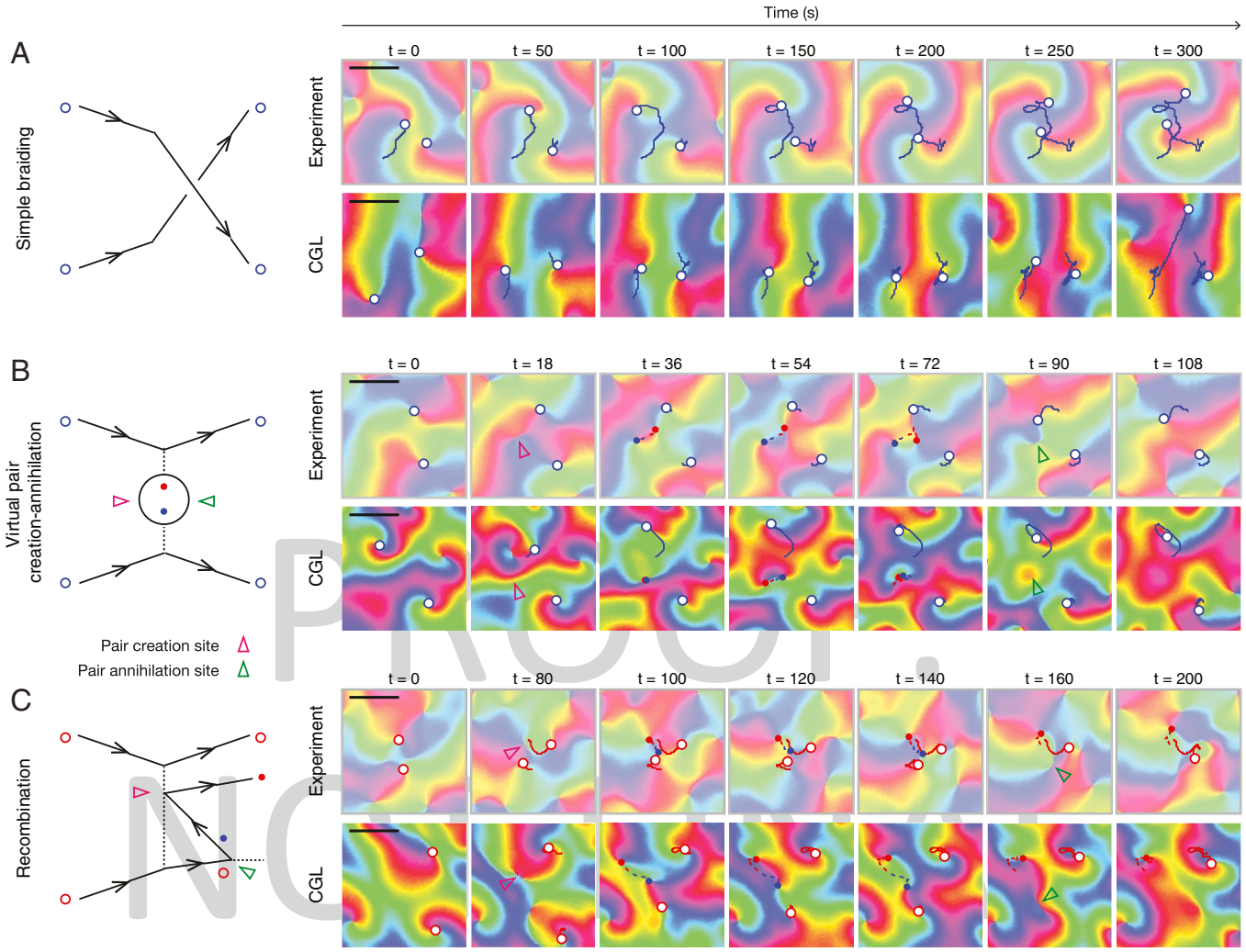

Fig. 5. Pair scattering events observed in experiments and simulations (*Right*), and their corresponding Feynman diagrams (*Left*). (*A*) Scattering event in which a pair of same-sign defects partially braids. From Movie S10: Time-lapse snapshots of an example event in experiment (*Upper*) and the CGL match (*Lower*). (Scale bar: 10 μm.) (*B*) Scattering event between two same-sign defects during which a short-lived "virtual" opposite-sign defect pair is created and annihilated. From Movie S10: Time-lapse snapshots of an example event in experiment (*Upper*) and the CGL match (*Lower*). (Scale bar: 10 μm.) (*C*) Scattering event during which a virtual defect pair is created and recombines with one of the incoming defects. From Movie S10: Time-lapse snapshots of an example event in experiment (*Upper*) and the CGL match (*Lower*). (Scale bar: 10 μm.)

during a 180° braiding operation determines the bosonic, fermionic, or anyonic nature of the fundamental excitations (25). Intriguingly, statistics of braiding defect pairs collected from the CGL states suggest a bosonic exchange symmetry (*SI Appendix*, Fig. S10) associated with the spiral wave system.

Defects as Organizers of Biophysical and Biochemical Signaling. Recent studies of eukaryotic cell layers (19, 28, 35) and bacterial colonies (18) revealed that topological defects play a central role in organizing collective cell dynamics (51), multicellular morphologies (34), and apoptosis (19). Similarly, topological defects at the centers of biochemical (52) and electrical spiral waves (13–16) have been shown to control the collective signaling in multicellular communities, including heart (13–15) and brain tissues (17). Providing an extension to signaling at the single-cell level, our above analysis suggests a link between ATP-driven cellular activity, spiral wave defect dynamics, and information flow on the oocyte membrane (Fig. 2). The eukaryotic Rho-GTP wave patterns studied here bear resemblance to bacterial Min protein oscillations (53), which similarly regulate mechanics during cell divisions (54) and can also realize spiral wave patterns under suitable conditions (55). From a theoretical perspective, the fact that key aspects of the Rho-GTP phase field dynamics can be captured by a generic CGL description (Fig. 4) further supports the hypothesis that topological defect analysis can provide a unifying framework for understanding robust information transport in biological systems. From an experimental perspective, an interesting next challenge is to decipher potential roles of the Rho-GTP membrane signaling defects in the organization of long-wavelength information during mitosis (45). Targeted optogenetic positioning of defects on the cell membrane may help answer this question in the near future.

Conclusions

Groundbreaking research over the last decade has identified topological defects as central organizers of biological information processing and function (17–19). Our analysis of the topological braiding dynamics in biochemical signaling waves on cell membranes demonstrates a framework for comparing information transport and processing in analogy with quantum systems. This paves the way for exploring whether recently developed optogenetic control techniques (23, 24) can enable the creation

and control of emergent bosonic, fermionic, or perhaps even anyonic excitations in biological matter.

Materials and Methods

Additional technical details of experiments and theoretical analysis are described in *SI Appendix*, which includes *SI Appendix*, Figs. S1–S10.

Data Acquisition. For this study, we combined data from previously reported measurements (22) of Rho-GTP steady-state wave patterns on *Patiria miniata* starfish oocyte membranes with data from newly performed experiments (Fig. 2) in which *P. miniata* starfish oocytes were treated with the ATP-depleting drug NaN_3 (sodium azide). In total, the data sets comprise five time series from ref. 22 and four time series from NaN_3 perturbed oocytes (Movie S8). All data were processed using a spectral representation method (*SI Appendix*) that enables previously unfeasible high-resolution phase-field reconstruction and dynamical analysis.

Starfish Oocyte Experiments. Oocytes were extracted from *P. miniata* starfish, washed by calcium-free seawater to prevent spontaneous maturation, and incubated at 15 °C. In vitro—synthesized messenger RNAs were prepared in the laboratory and delivered into cytoplasm via microinjection. Microscope imaging was performed after an overnight incubation to maximize protein expression in oocytes. For each experiment, 1-MA (1-methyl adenine) solution was used to induce meiosis. Fluorescent proteins were excited with a 488-nm laser, focused through a Nikon 60×/NA = 1.40 oil objective and collected using an EMCCD (electron multiplying charge coupling device) camera. The microscope room was maintained at 20 °C to 22 °C throughout the experiment. To obtain the data in Fig. 2, first, the meiosis process was induced until Rho-GTP spiral wave signaling patterns on membrane (time series I) reached a steady state, using the previous protocols (22) for acquiring steady-state data in Fig. 1. Then the oocytes were exposed to the ATP-depleting drug NaN_3 to obtain sequential time-lapse videos II, III, and IV as described in *SI Appendix* and shown in Movie S8.

CGL Simulations. The CGL equation (20),

$$\partial_t \psi = \psi - (1 + ic)|\psi|^2\psi + (1 + ib)\nabla^2\psi,$$

is a generic model describing the spatiotemporal evolution of oscillatory continuum systems $\psi(\mathbf{x}, t)$ near a Hopf bifurcation and can be quantitatively matched to a multispecies reaction—diffusion system (*SI Appendix*). Simulations of the CGL model were performed on a unit sphere using the MATLAB Chebfun library. Each simulation starts from a random initial condition and lasts for sufficient time to ensure decay of initial transient dynamics. A quantitative database and an interactive solver of spatiotemporal patterns of the CGL equation is available online at CGLE Atlas (49).

Data Availability. All data and analyses codes are available in *SI Appendix*. A quantitative database and an interactive solver of spatiotemporal patterns of the CGL equation are available online at CGLE Atlas, https://www.cgleatlas.com/ (49).

ACKNOWLEDGMENTS We thank Melis Tekant and Tzer Han Tan for their help in data acquisition. We thank Cristina Marchetti and Igor Aronson for helpful discussions, and Ned Wingreen for insightful comments. N.F. and J.D. are grateful to the Kavli Institute for Theoretical Physics program "ACTIVE20: Symmetry, Thermodynamics and Topology in Active Matter." This work was supported by a CAREER Award from NSF (N.F.), a Feodor Lynen Fellowship of the Alexander von Humboldt Foundation (J.F.T.), a Complex Systems Scholar Award from the James S. McDonnell Foundation (J.D.), and the Robert E. Collins Distinguished Scholarship Fund (J.D.). This research was supported, in part, by the NSF under Grant NSF PHY-1748958.

1. R. A. Naik, Failure analysis of woven and braided fabric reinforced composites. *J. Compos. Mater.* **29**, 2334–2363 (1995).
2. J.-L. Thiffeault, Measuring topological chaos. *Phys. Rev. Lett.* **94**, 084502 (2005).
3. A. Stern, N. H. Lindner, Topological quantum computation—From basic concepts to first experiments. *Science* **339**, 1179–1184 (2013).
4. H. Rossmanith, M. Doebroenti, M. Albach, D. Exner, Measurement and characterization of high frequency losses in nonideal litz wires. *IEEE Trans. Power Electron.* **26**, 3386–3394 (2011).
5. L. H. Kauffman, S. J. Lomonaco, Braiding, Majorana fermions, Fibonacci particles and topological quantum computing. *Quantum Inform. Process.* **17**, 201 (2018).
6. M. Budišić, J.-L. Thiffeault, Finite-time braiding exponents. *Chaos* **25**, 087407 (2015).
7. T. Bela Bauer *et al*., Topologically protected braiding in a single wire using Floquet Majorana modes. *Phys. Rev. B* **100**, 041102 (2019).
8. U. Tkalec, M. Ravnik, S. Čopar, S. Žumer, I. Muševič, Reconfigurable knots and links in chiral nematic colloids. *Science* **333**, 62–65 (2011).
9. S. Čopar, U. Tkalec, I. Muševič, S. Žumer, Knot theory realizations in nematic colloids. *Proc. Natl. Acad. Sci. U.S.A.* **112**, 1675–1680 (2015).
10. C. Nayak, S. H. Simon, A. Stern, M. Freedman, S. Das Sarma, Non-Abelian anyons and topological quantum computation. *Rev. Mod. Phys.* **80**, 1083–1159 (2008).
11. M. Freedman, A. Kitaev, M. Larsen, Z. Wang, Topological quantum computation. *Bull. Am. Math. Soc.* **40**, 31–38 (2003).
12. J. Lechleiter, S. Girard, E. Peralta, D. Clapham, Spiral calcium wave propagation and annihilation in *Xenopus laevis* oocytes. *Science* **252**, 123–126 (1991).
13. J. M. Davidenko, A. V. Pertsov, R. Salomonsz, W. Baxter, J. Jalife, Stationary and drifting spiral waves of excitation in isolated cardiac muscle. *Nature* **355**, 349–351 (1992).
14. R. A. Gray, A. M. Pertsov, J. Jalife, Spatial and temporal organization during cardiac fibrillation. *Nature* **392**, 75–78 (1998).
15. N. Bursac, F. Aguel, L. Tung, Multiarm spirals in a two-dimensional cardiac substrate. *Proc. Natl. Acad. Sci. U.S.A.* **101**, 15530–15534 (2004).
16. J. Christoph *et al*., Electromechanical vortex filaments during cardiac fibrillation. *Nature* **555**, 667–672 (2018).
17. X. Huang *et al*., Spiral wave dynamics in neocortex. *Neuron* **68**, 978–990 (2010).
18. K. Copenhagen, R. Alert, N. S. Wingreen, J. W. Shaevitz, Topological defects promote layer formation in *Myxococcus xanthus* colonies. *Nat. Phys.* **17**, 1–5 (2021).
19. T. B. Saw *et al*., Topological defects in epithelia govern cell death and extrusion. *Nature* **544**, 212–216 (2017).
20. I. S. Aranson, L. Kramer, The world of the complex Ginzburg-Landau equation. *Rev. Mod. Phys.* **74**, 99–143 (2002).
21. C. Brito, I. S. Aranson, H. Chaté, Vortex glass and vortex liquid in oscillatory media. *Phys. Rev. Lett.* **90**, 068301 (2003).
22. T. H. Tan *et al*., Topological turbulence in the membrane of a living cell. *Nat. Phys.* **16**, 657–662 (2020).
23. R. A. B. Burton *et al*., Optical control of excitation waves in cardiac tissue. *Nat. Photonics* **9**, 813–816 (2015).
24. R. Majumder *et al*., Optogenetics enables real-time spatiotemporal control over spiral wave dynamics in an excitable cardiac system. *eLife* **7**, e41076 (2018).
25. H. Bartolomei *et al*., Fractional statistics in anyon collisions. *Science* **368**, 173–177 (2020).
26. T. Sanchez, D. T. N. Chen, S. J. DeCamp, M. Heymann, Z. Dogic, Spontaneous motion in hierarchically assembled active matter. *Nature* **491**, 431–434 (2012).
27. S. J. DeCamp, G. S. Redner, A. Baskaran, M. F. Hagan, Z. Dogic, Orientational order of motile defects in active nematics. *Nat. Mater.* **14**, 1110–1115 (2015).
28. G. Duclos, C. Erlenkämper, J.-F. Joanny, P. Silberzan, Topological defects in confined populations of spindle-shaped cells. *Nat. Phys.* **13**, 58–62 (2017).
29. L. Giomi, M. J. Bowick, X. Ma, M. C. Marchetti, Defect annihilation and proliferation in active nematics. *Phys. Rev. Lett.* **110**, 228101 (2013).
30. S. Shankar, S. Ramaswamy, M. C. Marchetti, M. J. Bowick, Defect unbinding in active nematics. *Phys. Rev. Lett.* **121**, 108002 (2018).
31. F. Vafa, M. J. Bowick, M. C. Marchetti, B. I.Shraiman, Multi-defect dynamics in active nematics. arXiv [Preprint] (2020). https://arxiv.org/abs/2007.02947 (Accessed 24 May 2021).
32. A. Doostmohammadi, M. F. Adamer, S. P. Thampi, J. M. Yeomans, Stabilization of active matter by flow-vortex lattices and defect ordering. *Nat. Commun.* **7**, 10557 (2016).
33. S. Shankar, M. Cristina Marchetti, Hydrodynamics of active defects: From order to chaos to defect ordering. *Phys. Rev. X* **9**, 041047 (2019).
34. A. Doostmohammadi, S. P. Thampi, J. M. Yeomans, Defect-mediated morphologies in growing cell colonies. *Phys. Rev. Lett.* **117**, 048102 (2016).
35. C. Blanch-Mercader *et al*., Turbulent dynamics of epithelial cell cultures. *Phys. Rev. Lett.* **120**, 208101 (2018).
36. N. Kumar, R. Zhang, J. J. de Pablo, M. L. Gardel, Tunable structure and dynamics of active liquid crystals. *Sci. Adv.* **4**, eaat7779 (2018).
37. A. J. Tan *et al*., Topological chaos in active nematics. *Nat. Phys.* **15**, 1033–1039 (2019).
38. L. Braverman, C. Scheibner, V. Vitelli, Topological defects in non-reciprocal active solids with odd elasticity. arXiv [Preprint] (2021). https://arxiv.org/abs/2011.11543v2 (Accessed 24 May 2021).
39. M. C. Wigbers *et al*., A hierarchy of protein patterns robustly decodes cell shape information. *Nat. Phys.* **17**, 578–584 (2021).
40. A. U. Oza, J. Dunkel, Antipolar ordering of topological defects in active liquid crystals. *New J. Phys.* **18**, 093006 (2016).
41. J. Binysh, Ž. Kos, S. Čopar, M. Ravnik, G. P. Alexander, Three-dimensional active defect loops. *Phys. Rev. Lett.* **124**, 088001 (2020).
42. A. Piekny, M. Werner, M. Glotzer, Cytokinesis: Welcome to the Rho zone. *Trends Cell Biol.* **15**, 651–658 (2005).

43. Y. Fukata, M. Amano, K. Kaibuchi, K. Kaibuchi, Rho-Rho-kinase pathway in smooth muscle contraction and cytoskeletal reorganization of non-muscle cells. *Trends Pharmacol. Sci.* **22**, 32–39 (2001).
44. S. Etienne-Manneville, A. Hall, Rho GTPases in cell biology. *Nature* **420**, 629–635 (2002).
45. W. M. Bement *et al*., Activator-inhibitor coupling between Rho signalling and actin assembly makes the cell cortex an excitable medium. *Nat. Cell Biol.* **17**, 1471–1483 (2015).
46. C. N. Weiler *et al*., Spontaneous vortices in the formation of Bose–Einstein condensates. *Nature* **455**, 948–951 (2008).
47. T. Mawson, T. C. Petersen, J. K. Slingerland, T. P. Simula, Braiding and fusion of non-Abelian vortex anyons. *Phys. Rev. Lett.* **123**, 140404 (2019).
48. C. A. Abad, Introduction to representations of braid groups. *Rev. Colomb. de Mat.* **49**, 1–38 (2015).
49. J. F. Totz, CGLE Atlas. https://www.cgleatlas.com/ (Accessed 28 January 2021).
50. M. E. Peskin, *An Introduction to Quantum Field Theory* (CRC, Boca Raton, FL, 2018).
51. K. Kawaguchi, R. Kageyama, M. Sano, Topological defects control collective dynamics in neural progenitor cell cultures. *Nature* **545**, 327–331 (2017).
52. S. Sawai, P. A. Thomason, E. C. Cox, An autoregulatory circuit for long-range self-organization in *Dictyostelium* cell populations. *Nature* **433**, 323–326 (2005).
53. K. C. Huang, Y. Meir, N. S. Wingreen, Dynamic structures in *Escherichia coli*: Spontaneous formation of MinE rings and MinD polar zones. *Proc. Natl. Acad. Sci. U.S.A.* **100**, 12724–12728 (2003).
54. X. Yang *et al*., GTPase activity-coupled treadmilling of the bacterial tubulin FtsZ organizes septal cell wall synthesis. *Science* **355**, 744–747 (2017).
55. L. Wettmann, K. Kruse, The Min-protein oscillations in *Escherichia coli*: An example of self-organized cellular protein waves. *Phil. Trans. R. Soc. B* **373**, 20170111 (2018).